Green synthesized silver nanoparticles decorated on nanostructured porous silicon as an efficient platform for the removal of organic dye methylene blue

Nelson Naveas, Miguel Manso-Silván, Erico Carmona, Karla Garrido, Jacobo Hernández-Montelongo & Gonzalo Recio-Sánchez

Taylor & Francis
Taylor & Francis Group

RESEARCH LETTER

🔓 OPEN ACCESS ✅ Check for updates

Green synthesized silver nanoparticles decorated on nanostructured porous silicon as an efficient platform for the removal of organic dye methylene blue

Nelson Naveas[a,b], Miguel Manso-Silván[a,c], Erico Carmona[d], Karla Garrido[e], Jacobo Hernández-Montelongo[f] and Gonzalo Recio-Sánchez[g]

[a]Departamento de Física Aplicada and Instituto de Ciencia de Materiales Nicolás Cabrera, Universidad Autónoma de Madrid, Madrid, Spain; [b]Departamento de Ingeniería Química y Procesos de Minerales, Universidad de Antofagasta, Antofagasta, Chile; [c]Centro de Microanálisis de Materiales, Universidad Autónoma de Madrid, Madrid, Spain; [d]Facultad de Recursos Naturales, Universidad Arturo Prat, Iquique, Chile; [e]Center of Waste Management and Bioenergy, Scientific and Technological Bioresource Nucleus-BIOREN, Universidad de La Frontera, Temuco, Chile; [f]Departamento de Ciencias Matemáticas y Físicas, Universidad Católica de Temuco, Temuco, Chile; [g]Facultad de Ingeniería y Tecnología, Universidad San Sebastián, Concepción, Chile

ABSTRACT

In the present work, nanostructured porous silicon (nPSi) thin films were used as a substrate for the deposition of green synthesized silver nanoparticles (AgNPs). Different kinds of AgNPs were green synthesized by using *Peumo* extract and changing $AgNO_3$ concentration. UV-vis spectroscopy confirmed the success of the synthesis, and TEM characterization showed AgNPs with a like-spherical shape and an average diameter, which ranges from 4 to 25 nm, depending on the $AgNO_3$ concentration used. Then, AgNPs were introduced into the nPSi layer with a mean pore diameter of 46 nm and 75% of porosity by capillary suction. Hybrid layers nPSi/AgNPs were characterized by SEM, XRD, and RBS, confirming that AgNPs were introduced into nPSi layers. The catalytic activity of the hybrid layer in the reduction of organic dyes in water was studied using methylene blue (MB) as a model dye. Experimental results showed a high catalytic activity in comparison with other hybrid systems. The kinetic reduction could be fitted to the first-order equation obtaining the best degradation rate of 8.6 min^{-1} with AgNPs synthetized with 2 mM of $AgNO_3$. In addition, the reusability of these layers was demonstrated after five cycles, showing promising results for their use in wastewater management.
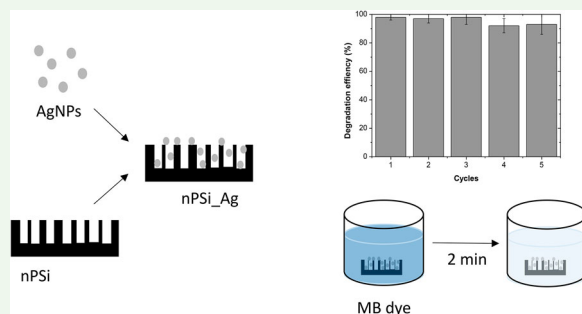
1. Introduction

During the last decade, metal nanoparticles have attracted the attention of the research community due to excellent plasmonic, antibacterial, and catalytic properties, among others [1,2]. Currently, there is a variety of commercial products that use metal nanoparticles, such as silver nanoparticles (AgNPs), and they are continuously being proposed for a massive of future applications [3]. Recently, green synthesis methods have become interesting routes to fabricate metal nanoparticles due to the ecofriendly and low cost of the process. In the green synthesis process, bacteria, fungi, or plant extracts can be used simultaneously as reducing and capping agents, without chemical agents or external energy consumption [4]. Biosynthesized AgNPs by plant extract have shown excellent antibacterial activities and catalytic activities for the reduction of organic dyes [5–7]. Moreover, they are being proposed for

CONTACT Gonzalo Recio-Sánchez ✉ gonzalo.recio@uss.cl 📱 Facultad de Ingeniería y Tecnología, Universidad San Sebastián, Lientur 1457, Concepción, Chile

further biomedical treatment to combat antibiotic-sensitive and multidrug-resistant strains such as *Pseudomonas aeruginosa* [8,9]. In addition, similar green synthesis routes are being explored to fabricate hybrid green materials with high potential for various therapeutic applications, including antibacterial and anti-inflammatory agents [10].

Currently, the bioaccumulation of organic dyes in wastewater has become one of the most serious environmental and human health issues. Several technologies have been developed to treat this problem such as membrane filtration, physical adsorption, and chemical degradation. However, catalytic degradation using metal nanoparticles has attracted much attention due to the efficiency of this process [11]. In this sense, green synthesized AgNPs have been demonstrated to be an appropriate alternative to reduce different organic dyes including methylene blue or rhodamine [12]. Nevertheless, the difficulty of recovering AgNPs from the aqueous solution for various cycles of reusing and their tendency to aggregate and decrease their catalytic activity are some disadvantages for the direct use of AgNPs in the wastewater management.

In this regard, the employment of appropriate substrates that host AgNPs can solve the problem of recovery of AgNPs to be utilized for several cycles and avoid the risk of bioaccumulation [13]. Different materials have been proposed for this goal including mesoporous materials such as zeolites or polymeric microspheres or others such as graphene [14–16]. In this context, nanostructured porous silicon (nPSi), which consists in a mesoporous structure of silicon nanocrystal, has been used as an efficient host material to incorporate metal nanoparticles and to obtain hybrid semiconductor–metal material [17].

In the present work, green synthesized AgNPs by using *Peumo* extract were directly deposited into the mesoporous nPSi layer by one-step capillary suction. Hybrid nPSi/AgNPs layers were physico-chemical characterized, and catalytic activity reduction of MB in water was investigated. Experimental results open the way to use this hybrid structure for organic dye wastewater treatment.

2. Materials and methods

2.1. Green synthesis of silver nanoparticles

The biosynthesis process of AgNPs was carried out by mixing an aqueous solution of $AgNO_3$ with previously prepared *Peumo* extract and stirring at room temperature. *Peumo* extract was prepared by adding 10 g of homogenized dried leaves and 200 mL of distilled water in a Soxhlet extractor for 4 h. Two different kinds of AgNPs were fabricated by changing the concentration of $AgNO_3$ and fixing the volume of *Peumo* extract at 1% v/v, following the previous work [18]. In this study, 1 and 2 mM concentrations of $AgNO_3$ were investigated, and the samples were named as Ag_1 mM and Ag_2 mM, respectively.

2.2. Fabrication of nanostructured porous silicon layer

nPSi thin films were fabricated by an electrochemical etching of crystalline p$^+$ type boron-doped silicon wafers (orientation <100>; low resistivity $\rho = 0.001–0.005$ Ω·cm) in HF (48% wt): ethanol (96% wt) (1:2) solutions. Hence, silicon wafers were cut into pieces of 2.5 cm × 2.5 cm and were placed on a hand-made Teflon electrochemical cell, with a spherical area of 2 cm of diameter to expose to the electrolyte. The applied current density was 80 mA/cm^2 during 5 min to obtain nPSi layer of 10 μm of thickness and average porosity around 75% [17].

2.3. Fabrication of hybrid nPSi-Ag layers

Once nPSi layers were fabricated, Ag nanoparticles were incorporated into the porous matrix by capillary suction, dropping a total of 3 ml of ethanol solution of 1 mg/ml concentration of Ag nanoparticles and stirring at 60 rpm at room temperature until the last drop is dried. Then, samples were washed with ethanol, dried, and stored. Two kinds of hybrid layers were fabricated by changing the type of AgNPs used. One sample was named as nPSi_Ag_1 mM if Ag_1 mM nanoparticles were used. The other sample was named as nPSi_Ag_2 mM, where Ag_2 mM was incorporated.

2.4. Physico-chemical characterization

UV-visible absorption measurements were performed with a Shimadzu spectrophotometer (UV-mini 1240 model). Absorption measurements of AgNPs were recorded with an integration time of 0.1 s and an interval of 1 nm, in the range from 300 to 750 nm. UV-vis absorption spectra for MB degradation were measured on very fast speed mode with a scan rate of 1400 nm/min, in the range from 550 to 750 nm.

AgNPs morphology was studied by transmission electron microscopy (JEOLJEM-2011 instrument), and images were analyzed by ImageJ software. Morphological characterizations of the nPSi layers and hybrid nPSi_Ag layers were studied by field-emission scanning electron microscopy (SEM FEI VERIOS 460), operating with an acceleration potential of 2 keV.

X-ray diffraction measurements were carried out with a Rigaku X-ray diffractometer (Smartlab model), using a Theta-Theta Bragg–Brentano goniometer and a solid-state detector (D/text Ultra 250 model) and with Ni filtered Cu radiation operating at 30 kV and 40 mA.

Rutherford Backscattering Spectroscopy (RBS) experiments were conducted at the standard beamline at the 5 MV Cockroft–Walton tandetron accelerator of the Centro de Micro-Análisis de Materiales (CMAM). For the measurements, 2 MeV He+ ions were used. The scattered ions were detected at a scattering angle of 170° with an Si semiconductor particle detector; samples were oriented in random geometry to avoid channeling through the crystalline substrate. The vacuum was about 5×10^{-5} Pa. Spectra fitting was carried out using software SIMNRA 7.02.

2.5. Reduction of MB dye

Catalytic reduction experiments of MB were carried out by immersing the final silicon-based piece of 2.5 cm × 2.5 cm containing the nPSi-Ag layer into 20 ml of dye solution (3.1×10^{-5} M MB and 0.003 M $NaBH_4$). UV-vis absorption spectra were recorded at different times to monitor the progress of the reaction. As a control, the same process was carried out with a pristine nPSi layer. After each removal (2 min), the sample was removed with tweezers, washed with distilled water, and reimmersed into a 10 ml of fresh dye solution. The process was repeated with five different samples, and statistical analysis was performed.

The percentage of reduction of MB (RE_{MB}) was obtained by the following equation:

$$RE_{MB} = \frac{C_o - C_f}{C_o} \cdot 100\% \qquad (1)$$

where C_o and C_f are the initial concentration of MB and the final concentration, respectively. The initial and final concentrations were measured by UV-vis spectroscopy at a wavelength of 664 nm.

3. Results and discussion

The biosynthesis process of AgNPs was characterized by UV-vis spectroscopy. Figure 1 shows the absorption spectrum of *Peumo* extract with the absorption spectra of AgNPs recorded after 24 h of reaction (Ag_1 mM and Ag_2 mM are referred to as two different kinds of AgNPs, see experimental details for further information). It can be observed that *Peumo* extract has a wide band centered at 340 nm, which is related to the absorption of biocompound that forms the extract. After reducing Ag salt, AgNPs have an absorption peak centered at
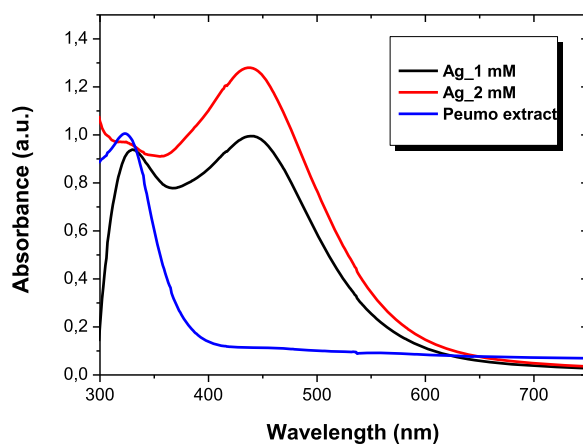

Figure 1. UV-vis absorption spectra of AgNPs biosynthesized with different concentrations of $AgNO_3$ and aqueous *Peumo* extract.

445 nm related to the localized surface plasmon resonance of AgNPs, confirming the success of the process.

Figure 2 shows TEM images of AgNPs. It can be observed that Ag_1 mM (Figure 2(a)) presents a spherical-like shape and very small size, with an average diameter of 4.3 ± 2.1 nm. However, they tend to agglomerate as was expected for this kind of nanoparticles. Conversely, Ag_2 mM also shows a spherical-like shape with an average diameter of 25 ± 3 nm, providing them higher stability. Similar morphologies have been obtained by using other kinds of plant extracts. *Lysiloma acapulcensis* extract was able to form spherical-like AgNPs with 5 nm of diameter, and other medicinal plant such as *Eucalyptus globulus* or *Abutilon indicum* can synthesize AgNPs with average diameter ranging from 5 to 25 nm [19,20].

After AgNPs were synthesized, nPSi layers were fabricated. Figure 3(a) shows an SEM image of the nPSi layer used in this study. As shown earlier, the nPSi surface is characterized by a homogeneous pore distribution with a mean pore diameter of 46 ± 7 nm. Figure 3(b,c) show the surface of hybrid layer nPSi_Ag_1 mM and nPSI_Ag_2 mM, respectively, after deposition of biosynthesized AgNPs by simple capillary suction. Sample nPSi-Ag-1 mM shows aggregates of more than 100 nm on the surface of the nPSi layer. This fact confirms the tendency to agglomerate by this kind of AgNPs during the deposition process. On the other hand, sample nPSi-Ag-2 mM only shows some aggregates on the surface, suggesting that most AgNPs were incorporated inside the porous structure.

Figure 4 shows the XRD patterns of each sample. The nPSi layer shows four different diffraction peaks centered at 33.07°, 47.56°, 54.41°, and 56.68°, which correspond to (2 0 0), (2 2 0), (1 2 0), and (3 1 1)
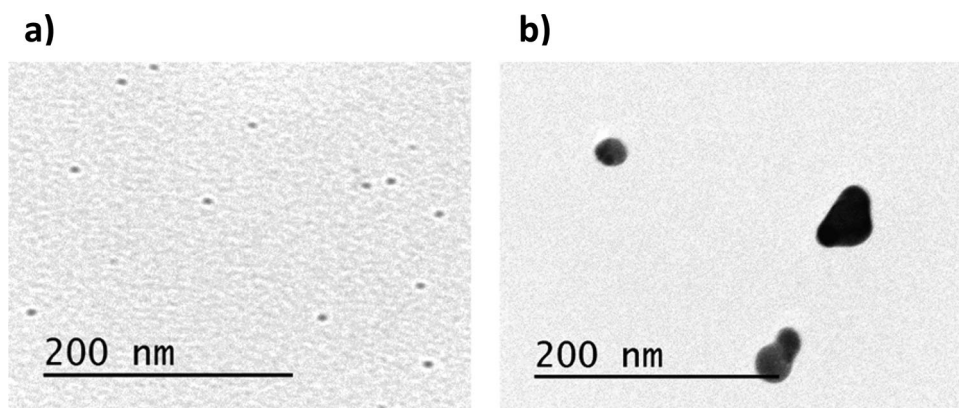
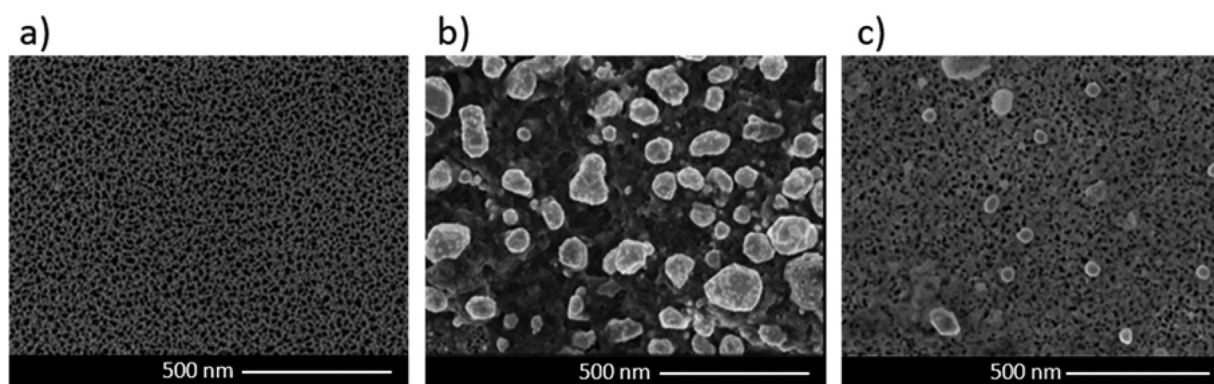**Figure 2.** TEM images of (a) Ag_1 mM and (b) Ag_2 mM

Figure 3. SEM images of (a) nPSi surface, (b) nPSi_Ag_1 mM surface, and (c) nPSi_Ag_2 mM.

crystallographic planes of Si structure, respectively. Conversely, both kinds of AgNPs show two diffraction peaks at 38.28° and 44.40°, which correspond to (1 1 1) and (2 0 0) lattice planes of metallic cubic silver, respectively, according to ICDD PDF card 03-065-2871, confirming the crystalline nature of the AgNPs. Furthermore, in nPSi_Ag_1 m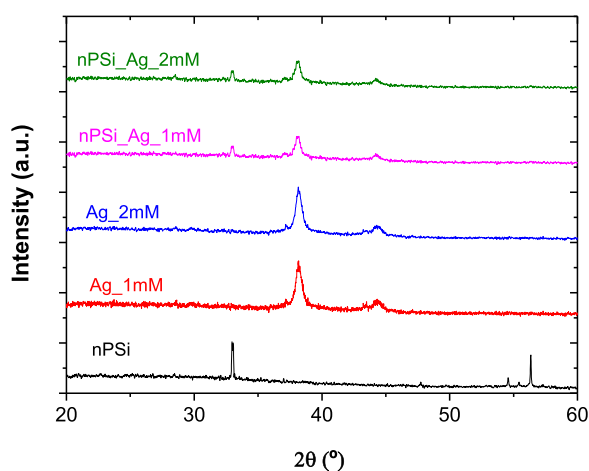M and nPSi_Ag_2 mM diffraction patterns, three diffraction peaks can be observed. One at 33.07° related to the nPSi layer, and the other two at 38.28° and 44.40° concerning to the AgNPs, as it was expected.

RBS was used to study the infiltration of AgNPs into the nPSi layer. Figure 5 shows the experimental and simulated RBS spectra of nPSi_Ag_1 mM and nPSi_Ag_2 mM hybrid layers. While the signals corresponding to Ag and Si are clearly differentiated in both spectra, the O signal appears superimposed to the Si signal. Both samples show a higher Ag signal at the top of the surface, extending from its surface position to lower energy channels, indicating that Ag is infiltrated into the nPSi layer.

Figure 6 shows the in-depth concentration profile determined from the fitted spectra. As it is expected, oxygen concentration decreases in depth for both samples. The presence of oxygen is given by the high reactivity of the nPSi surface, which tends to rush with the contact of the atmosphere and during the process of AgNPs infiltration. As oxygen concentration decreases, Si concentration increases in depth. Moreover, the profiles show the presence of Ag on the surface of nPSi layers and into the porous structures. According to SEM images, Ag concentration on the
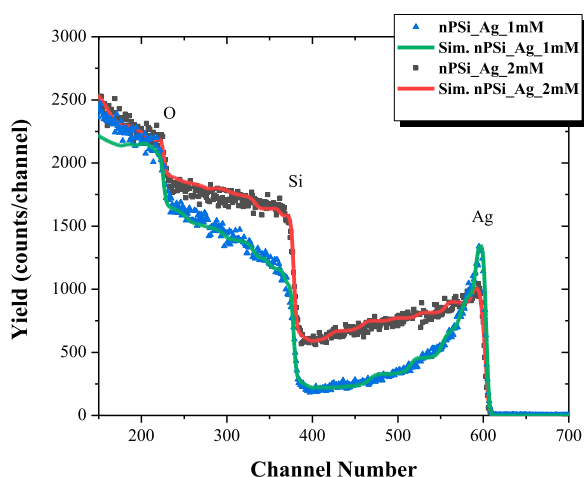

Figure 4. XRD patterns of nPSi layer, AgNPs and nPSi_Ag_1 mM, and nPSi_Ag_2 mM samples.

Figure 5. RBS spectra of nPSi_Ag_1 mM and nPSi_Ag_2 mM.

surface of nPSi was higher in nPSi_Ag_1 mM (Figure 6(a)) than in the nPSi_Ag_2 mM sample (Figure 6(b)). However, the Ag signal quickly diminishes for the first sample confirming that Ag_1 mM tends to accumulate on the surface of the nPSi layer and just a low quantity diffuses into the porous layer. Conversely, for the nPSi_Ag_2 mM sample, a lower concentration of Ag is obtained on the surface of the nPSi layer. However, the signal slowly decreases in depth, hinting at the higher quantity of AgNPs incorporated into the porous structure [21].

The catalytic activity of hybrid layer nPSi_Ag was studied using MB as model organic dye. nPSi layers were introduced into 10 ml of dye solution (3.1×10^{-5} M MB and 0.003 M NaBH$_4$), and the degradation of MB was followed by UV-vis spectroscopy. In the presence of NaBH$_4$, MB can be reduced to uncolored Leuco-MB [18]. Here,

NaBH$_4$ acts as a reductor agent for the oxidated state of MB. Figure 7(a) shows the UV-vis absorption spectra of dye solution recorded at different time periods when the pristine nPSi layer was introduced. The main spectrum of MB was characterized by a wide absorption band between 550 and 700 nm, with two main peaks at 604 and 664 nm. After 30 min, just 11.8% of MB was reduced. In contrast, hybrid nPSi_Ag layers highly increase the degradation rate. nPSi_Ag_1 mM was able to completely degrade MB over a minute (Figure 7(b)). Conversely, MB was effectively degraded in less than 30 s using nPSi_Ag_2 mM hybrid layers (Figure 7(c)).

The kinetic reduction of each layer was fitted to the first-order equation: $Ln(A_0/A_i) = kt$, where A_0 is the initial absorbance at 664 nm, A_i is the absorbance at 664 nm at any time, k is the degradation rate, and t is the time. The main values are presented in Table 1. For all the samples explored in this study, the degradation rate can be well fitted to the first-order kinetic. For the pristine nPSi layer, a low k rate constant value of 0.00183 min^{-1} was obtained, suggesting that the nPSi layer did not show any catalytic activity. Hybrid nPSi_Ag layers dramatically increased the k rate constant to 3.8 and 8.6 min^{-1} for nPSi_Ag_1 mM and nPSi_Ag_2 mM, respectively, due to the high catalytic activity of AgNPs.

The degradation rate of nPSi_Ag layers was compared to other similar works in Table 2. It can be observed that nPSi_Ag hybrid layers shows a high degradation rate compared to with other platforms, indicating its promising utilization in wastewater dye treatment. However, the degradation rate of MB depends on several parameters such as MB concentration, amount of catalyst used, temperature, and pH,
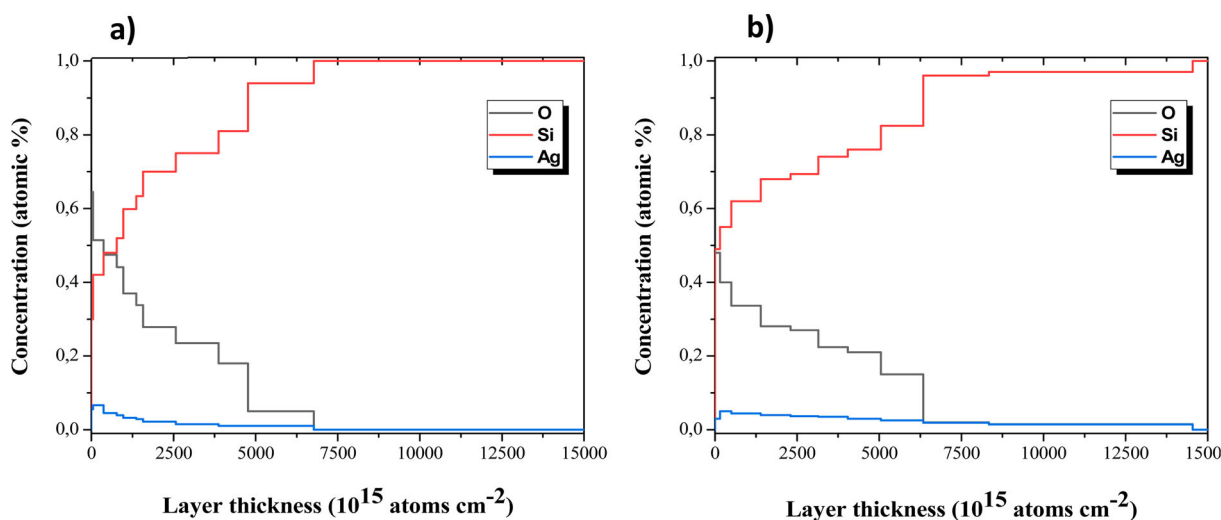

Figure 6. In-depth concentration profile of RBS simulation for (a) nPSi_Ag_1 mM and (b) nPSi_Ag_2 mM.
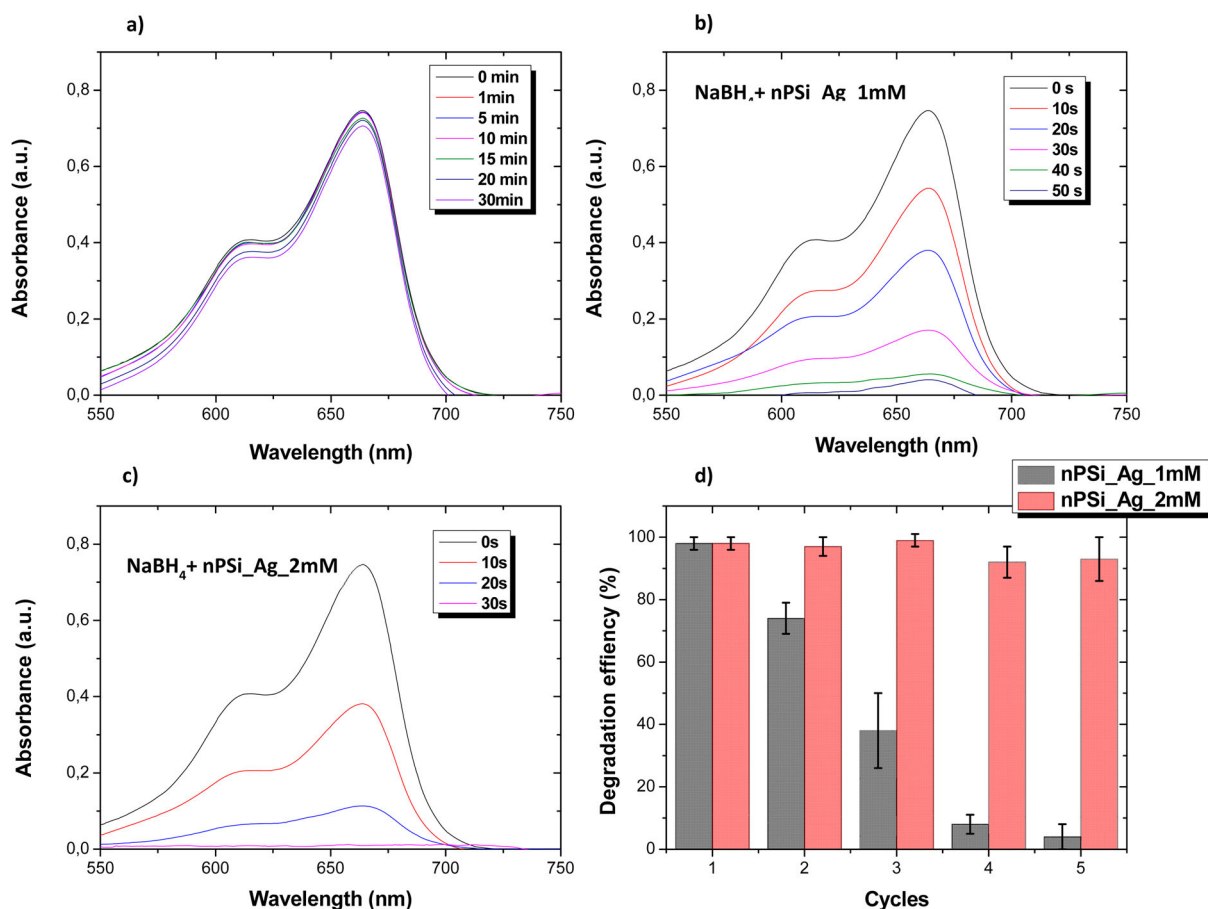
Figure 7. UV-vis spectra of dye solution recorded at different time periods under the exposition to (a) pristine nPSi layer, (b) nPSi_Ag_1 mM layer, and (c) nPSi_Ag_2 mM sample. (d) Reusability experiment over five cycles of the degradation of MB using nPSi_Ag hybrid layer as a catalyst.

among others. Thus, further studies in similar conditions should be done.

The reusability of these structures was also investigated. For that, the degradation efficiency was calculated after 2 min of immersion into the dye solution. This time was set to ensure the reduction of MB during the first cycle. Then, hybrid layers were removed, washed with distilled water, and reimmersed in a fresh dye solution. Experiments were carried out with five different samples, and experimental results are summarized in Figure 7(d). nPSi_Ag_2 mM are able to degrade MB solutions after five cycles without almost losing their efficiency. In contrast, nPSi_Ag_1 mM layers clearly reduced their efficiency after the first cycle.

Results suggest that the tendency to bioaccumulate Ag_1 mM on the surface of the nPSi layer reduces its active size to catalyze the degradation of MB compared to Ag_2 mM. Moreover, it seems that the Ag_1 mM is inclined to release into the aqueous medium, showing less stability than Ag_2 mM. Thus, the catalytic activity of nPSi_Ag_1 mM is rapidly decreased after the first cycle in comparison to nPSi_Ag_2 mM, where Ag

Table 1. Kinetic first-order parameters of degradation of MB using nPSi_Ag layers.

Sample	k value (min^{-1})	R^2
Pristine nPSi	0.00183 ± 0.00006	0.998
nPSi_Ag_1 mM	3.8 ± 0.4	0.989
nPSi_Ag_2 mM	8.6 ± 0.9	0.991

Table 2. Comparison of catalytic degradation of MB using AgNPs on different substrates.

Catalyst	Pollutant	Degradation rate	Reference
Fe$_3$O$_4$@PS@Ag	MB 5×10^{-5} M	0.0089 s^{-1}	[16]
Fe$_3$O$_4$@SiO$_2$/Ag	MB 5×10^{-5} M	1.58 min^{-1}	[22]
ZnO-Ag	MB 20 ppm	90% in 180 min	[23]
Cotton-Ag	MB 10 mg/L	>99% in 24 h	[24]
Ag@WO$_3$/GO	MB 10 ppm	0.296 min^{-1}	[25]
AgNPs/g-C$_3$N$_4$	MB 1×10^{-5} M	0.395 min^{-1}	[26]
ZnO-Ag	MB 5 mg/L	>99% in 75 min	[27]
Ag/Fe$_3$O$_4$@GO	MB- 5×10^{-5} M	0.448 min^{-1}	[28]
NC-AgNPs	MB 0.15 mM	0.151 min^{-1}	[29]
rGO/PDA-2/Ag-15	MB 10 ppm	>99% in 60 min	[30]
nPSi_Ag_2mM	**MB 3.1×10^{-5} M**	**8.6 min^{-1}**	**This work**

nanoparticles are incorporated into the porous structure of the nPSi matrix.

4. Conclusion

Green synthesized Ag nanoparticles using *Peumo* extract were successfully incorporated into nPSi by one-step capillary suction. Final properties of nPSi_Ag hybrid structure depend on the main characteristic of Ag nanoparticles, which can be controlled by changing the Ag salt concentration during its synthesis. AgNPs tend to accumulate on the surface of the nPSi layer, but they were also introduced into the porous structure. The catalytic activity of nPSi_Ag platforms was demonstrated. They were able to degrade MB in the presence of $NaBH_4$ with a high degradation rate in comparison with other similar works. Moreover, hybrid layers were easily recovered and used for several cycles without losing their efficiency, showing that nPSi is a promising substrate for AgNPs.

Disclosure statement

No potential conflict of interest was reported by the author(s).

References

[1] Tighe-Neira, R.; Carmora, E.; Recio, G.; Nunes-Nesi, A.; Reyes-Diaz, M.; Alberdi, M.; Rengel, Z.; Inostroza-Blancheteau, C. Metallic Nanoparticles Influence the Structure and Function of the Photosynthetic Apparatus in Plants. *Plant Physiol. Biochem.* **2018**, *130*, 408–417. doi:10.1016/j.plaphy.2018.07.024

[2] Ndolomingo, M.J.; Bingwa, N.; Meijboom, R. Review of Supported Metal Nanoparticles: Synthesis Methodologies, Advantages and Application as

[3] Tufail, M.S.; Liaqat, I. Silver Nanoparticles and Their Applications-A Comprehensive Review. *Pure Appl. Biol.* **2021**, *11* (1), 315–330.

[4] Rana, A.; Yadav, K.; Jagadevan, S. A Comprehensive Review on Green Synthesis of Nature-Inspired Metal Nanoparticles: Mechanism, Application and Toxicity. *J. Clean. Prod.* **2020**, 272, 122880. doi:10.1016/j.jclepro. 2020.122880

[5] Carmona, E.R.; Benito, N.; Plaza, T.; Recio-Sánchez, G. Green Synthesis of Silver Nanoparticles by Using Leaf Extracts from the Endemic Buddleja Globosa Hope. *Green Chem. Lett. Rev.* **2017**, *10* (4), 250–256. doi:10. 1080/17518253.2017.1360400

[6] Molina, G.A.; Esparza, R.; López-Miranda, J.L.; Hernández-Martínez, A.R.; España-Sánchez, B.L.; Elizalde-Peña, E.A.; Estevez, M. Green Synthesis of Ag Nanoflowers Using Kalanchoe Daigremontiana Extract for Enhanced Photocatalytic and Antibacterial Activities. *Colloids Surf. B* **2019**, *180*, 141–149. doi:10. 1016/j.colsurfb.2019.04.044

[7] Jin, Y.; Li, B.; Saravanakumar, K.; Hu, X.; Mariadoss, A.V.A.; Wang, M.H. Cytotoxic and Antibacterial Activities of Starch Encapsulated Photo-Catalyzed Phytogenic Silver Nanoparticles from Paeonia Lactiflora Flowers. *J. Nanostructure Chem.* **2021**, 1–13.

[8] Habibipour, R.; Moradi-Haghgou, L.; Farmany, A. Green Synthesis of AgNPs@ PPE and its *Pseudomonas aeruginosa* Biofilm Formation Activity Compared to Pomegranate Peel Extract. *Int. J. Nanomed.* **2019,** *14*, 6891–6899. doi:10.2147/IJN.S209912

[9] de Lacerda Coriolano, D.; de Souza, J.B.; Bueno, E.V.; Medeiros, S.; Cavalcanti, I.L.; Cavalcanti, I. Antibacterial and Antibiofilm Potential of Silver Nanoparticles Against Antibiotic-Sensitive and Multidrug-Resistant Pseudomonas Aeruginosa Strains. *Braz. J. Microbiol.* **2021**, *52* (1), 267–278. doi:10.1007/s42770-020-00406-x

[10] Asghar, M.A.; Yousuf, R.I.; Shoaib, M.H.; Asghar, M.A.; Zehravi, M.; Rehman, A.A.; Imtiaz, M.S.; Khan, K. Green Synthesis and Characterization of Carboxymethyl Cellulose Fabricated Silver-Based Nanocomposite for Various Therapeutic Applications. *Int. J. Nanomed.* **2021,** *16*, 5371–5393. doi:10.2147/IJN.S321419

[11] Jain, K.; Patel, A.S.; Pardhi, V.P.; Flora, S.J.S. Nanotechnology in Wastewater Management: A New Paradigm Towards Wastewater Treatment. *Molecules* **2021,** *26* (6), 1797. doi:10.3390/molecules26061797

[12] Goutam, S.P.; Saxena, G.; Roy, D.; Yadav, A.K.; Bharagava, R.N. Green Synthesis of Nanoparticles and Their Applications in Water and Wastewater Treatment. In *Bioremediation of Industrial Waste for Environmental Safety*; Springer: Singapore, **2020**; 349–379. doi: 10. 1007/978-981-13-1891-7_16.

[13] Sarkar, D.; Khare, D.; Kaushal, A.; Acharya, C.; Bahadur, J.; Prakash, J.; Donthula, H.; Dasgupta, K. Green and Scalable Synthesis of Nanosilver Loaded Silica Microparticles by Spray-Drying: Application as Antibacterial Agent, Catalyst and SERS Substrate. *Appl. Nanosci.* **2019**, *9* (8), 1925–1937. doi:10.1007/s13204-019-01031-3

Catalysts. *J. Mater. Sci.* **2020**, *55* (15), 6195–6241. doi:10.1007/s10853-020-04415-x

[14] Huang, Y.B.; Wang, Q.; Liang, J.; Wang, X.; Cao, R. Soluble Metal-Nanoparticle-Decorated Porous Coordination Polymers for the Homogenization of Heterogeneous Catalysis. *J. Am. Chem. Soc* **2016**, *138* (32), 10104–10107. doi:10.1021/jacs.6b06185

[15] Deng, C.H.; Gong, J.L.; Zhang, P.; Zeng, G.M.; Song, B.; Liu, H.Y. Preparation of Melamine Sponge Decorated with Silver Nanoparticles-Modified Graphene for Water Disinfection. *J. Colloid Interface Sci*. **2017,** *488*, 26–38. doi:10.1016/j.jcis.2016.10.078

[16] Wang, Y.; Gao, P.; Wei, Y.; Jin, Y.; Sun, S.; Wang, Z.; Jiang, Y. Silver Nanoparticles Decorated Magnetic Polymer Composites (Fe3O4@ PS@ Ag) as Highly Efficient Reusable Catalyst for the Degradation of 4-Nitrophenol and Organic Dyes. *J. Environ. Manage*. **2021**, *278*, 111473. doi:10.1016/j.jenvman.2020.111473

[17] Hernández-Montelongo, J.; Fernández-Fierro, C.; Benito-Gómez, N.; Romero-Sáez, M.; Parodi, J.; Carmona, E.R.; Recio-Sánchez, G. Hybrid Porous Silicon/Green Synthetized Ag Microparticles as Potential Carries for Ag Nanoparticles and Drug Delivery. *Mater. Sci. Eng. C* **2020,** *116*, 111183. doi:10.1016/j.msec.2020.111183

[18] Recio-Sánchez, G.; Tighe-Neira, R.; Alvarado, C.; Inostroza-Blancheteau, C.; Benito, N.; García-Rodríguez, A.; Marcos, R.; Pesenti, H.; Carmona, E.R. Assessing the Effectiveness of Green Synthetized Silver Nanoparticles with Cryptocarya Alba Extracts for Remotion of the Organic Pollutant Methylene Blue dye. *Environ. Sci. Pollut. Res*. **2019**, *26* (15), 15115–15123. doi:10.1007/s11356-019-04934-4

[19] Garibo, D.; Borbón-Nuñez, H.A.; de León, J.N.D.; Mendoza, E.G.; Estrada, I.; Toledano-Magaña, Y.; Tiznado, H.; Ovalle-Marroquin, M.; Soto-Ramos, A.; Rodríguez, J.A.; Romo, O.A.; Chávez-almazán, L.A.; Susarrey-Arce, A. Green Synthesis of Silver Nanoparticles Using Lysiloma Acapulcensis Exhibit High-Antimicrobial Activity. *Sci. Rep*. **2020**, *10* (1), 1–11. doi:10.1038/s41598-020-69606-7

[20] Ahmed, R.H.; Mustafa, D.E. Green Synthesis of Silver Nanoparticles Mediated by Traditionally Used Medicinal Plants in Sudan. *Int. Nano. Lett*. **2020**, *10* (1), 1–14. doi:10.1007/s40089-019-00291-9

[21] Naveas, N.; Manso-Silván, M.; Pulido, R.; Agulló-Rueda, F.; Torres-Costa, V.; Plaza, T.; Pesenti, H.; Recio-Sánchez, G.; Hernández-Montelongo, J. Fabrication and Characterization of Nanostructured Porous Silicon-Silver Composite Layers by Cyclic Deposition: Dip-Coating vs Spin-Coating. *Nanotechnology* **2020**, *31* (36), 365704.

[22] Chishti, A.N.; Ni, L.; Guo, F.; Lin, X.; Liu, Y.; Wu, H.; Chen, M.; Diao, G.W. Magnetite-Silica Core-Shell Nanocomposites Decorated with Silver Nanoparticles for Enhanced Catalytic Reduction of 4-Nitrophenol and Degradation of Methylene Blue dye in the Water. *J. Environ. Chem. Eng*. **2021**, *9* (2), 104948. doi:10.1016/j.jece.2020.104948

[23] Al-Gharibi, M.A.; Kyaw, H.H.; Al-Sabahi, J.N.; Myint, M.T.Z.; Al-Sharji, Z.A.; Al-Abri, M.Z. Silver Nanoparticles Decorated Zinc Oxide Nanorods Supported Catalyst for Photocatalytic Degradation of Paracetamol. *Mater. Sci. Semicond. Process* **2021**, *134*, 105994. doi:10.1016/j.mssp.2021.105994

[24] El-Naggar, M.E.; Khattab, T.A.; Abdelrahman, M.S.; Aldalbahi, A.; Hatshan, M.R. Development of Antimicrobial, UV Blocked and Photocatalytic Self-Cleanable Cotton Fibers Decorated with Silver Nanoparticles Using Silver Carbamate and Plasma Activation. *Cellulose* **2021,** *28* (2), 1105–1121. doi:10.1007/s10570-020-03537-4

[25] Abd Elhakim, A.; El-Kemary, M.; Ibrahim, M.M.; El-Mehasseb, I.M.; EL-Sheshtawy, H.S. Direct Z-Scheme of WO3/GO Decorated with Silver Nanoparticles for Synergetic Adsorption and Photocatalytic Activity for Organic and Inorganic Water Pollutants Removal. *Appl. Surf. Sci*. **2021**, *564*, 150410. doi:10.1016/j.apsusc.2021.150410

[26] Murugan, E.; Santhoshkumar, S.; Govindaraju, S.; Palanichamy, M. Silver Nanoparticles Decorated g-C3N4: An Efficient SERS Substrate for Monitoring Catalytic Reduction and Selective Hg2 + Ions Detection. *Spectrochim. Acta A Mol. Biomol. Spectrosc*. **2021**, *246*, 119036. doi:10.1016/j.saa.2020.119036

[27] Jadhav, P.; Shinde, S.; Suryawanshi, S.S.; Teli, B.; Patil, P.S.; Ramteke, A.A.; Hiremath, N.G.; Prasad, N.R. Green AgNPs Decorated ZnO Nanocomposites for dye Degradation and Antimicrobial Applications. *Eng. Sci*. **2020**, 79–94. doi:10.30919/es8d1138

[28] Doan, V.D.; Nguyen, N.V.; Nguyen, T.L.H.; Tran, V.A. High-efficient Reduction of Methylene Blue and 4-Nitrophenol by Silver Nanoparticles Embedded in Magnetic Graphene Oxide. *Environ. Sci. Pollut. Res*. **2021**, 1–11. doi:10.1007/s11356-021-13597-z.

[29] Edison, T.N.J.I.; Atchudan, R.; Karthik, N.; Balaji, J.; Xiong, D.; Lee, Y.R. Catalytic Degradation of Organic Dyes Using Green Synthesized N-Doped Carbon Supported Silver Nanoparticles. *Fuel* **2020,** *280*, 118682. doi:10.1016/j.fuel.2020.118682

[30] Qian, Y.; Zhou, C.; Zhou, J.; Huang, A. Synthesis of Silver-Nanoparticles Composite with Highly Catalytic Activity Supported on the Reduced Graphene Oxide. *Appl. Surf. Sci* **2020**, *525*, 146597. doi:10.1016/j.apsusc.2020.146597